# Interface Locking of Subduction Zone near Costa Rica using Seismic and Geodetic Methods

Yan Luo

School of Earth and Atmospheric Sciences, Georgia Institute of Technology, Atlanta, GA, 30332

**Abstract**

Most of the world's largest earthquakes occur along subduction megathrusts. Study of the evolution mechanism of seismogenic locking and strain accumulation along the subducting interface is crucial for estimating recurrence of these destructive events. The Costa Rica region is ideal for investigating megathrust earthquakes because of the region's proximity to the subducting interface and abundance of existing and new seismic and geodetic data.

For this project, I have manually located more than 5000 local earthquakes that occurred in 2009 in the Costa Rica region by using the Antelope seismic analysis software. I have applied the local magnitudes of these events to demonstrate the spatial variability of frequency-magnitude (FM) along the subduction interface of the Nicoya Peninsula. Preliminary results show the current spatial FM distribution has changed compared with Nicoya seismicity FM (between late-1999 and mid-2001) maps produced by previous studies. This change is most likely due to either slow slip events or tremor, or a variation in an interface property.

Future work includes generating a best-fit 3-D interface model for the Costa Rican subduction zone by using the seismicity distribution along the approximate interface. I will then use the geometry of this newly generated subduction interface model, combining with GPS surface deformation data (from 1996 to 2010) of the Nicoya Peninsula, to generate the inversion results of the slip distribution along the interface.

This analysis can be used as a good proxy for locating accumulated stress along the megathrust interface. If the simulated interface model works well, I will also apply it to specifically examine the stress accumulation pattern changes before and after the 2007 slow slip event by calculating the inversion results of GPS movement data. I will then evaluate the impact of slow slip events on potential regions of future megathrust earthquakes with highly accumulated stress.

## Introduction

### 1.Overview and Motivation

Earthquake activities usually occur along the plate boundaries, which comprise conservative, divergent and convergent boundaries. Especially, subduction zones, typical regions of convergent boundary, create the majority of large earthquakes ($Mw$>8.0). It is because the subduction zones have large area of lithospheric plates sliding against each other, and negative buoyancy force drives this plate consuming process ceaselessly. Globally, 80 percentage of the global seismic moment was released around those subduction seismogenic zones [*Pacheco & Sykes,* 1992]. Great shaking of the ground produced by these megathrust earthquakes and tsunami caused by the failure of shallow portion of the subduction interface have been inducing dramatically and catastrophically hazards to coastal population. Hence, it is very important to investigate the evolution of interface locking, which is the process that the fault strength is accumulated on the subduction interface due to shear stress transfer, to study on how the earthquakes associate with the interface locking, and to evaluate the possible influence of other tectonic phenomena on the interface locking, such as non-volcanic tremor, slow slip event, etc.

In this study, I choose Costa Rica region, because the Nicoya Peninsula of Costa Rica is proximal to the Middle America Trench (MAT). Besides, abundance of existing geodetic and seismic data also provides excellent foundation for this research. Earthquake catalog of this region in 2009 is used to check the spatial and temporal variation of frequency of seismicity magnitude distribution, and then I verify that if the seismicity rate distribution can be used as a proxy of interface locking underneath Nicoya. In addition, geodetically, Global Positioning Systems (GPS) data from four field Campaigns (1996 to 2010) and continuous GPS sites, and 3-D slab model

defined by the micro-seismicities will also be used for this study. Combining tools of geodetic and seismological methods, I will try to enhance our understanding on the process of subduction interface locking, and its interactions with seismicity and other tectonic phenomena.

**2. Tectonic setting**

Nicoya Peninsula offshore is close to the MAT with approximate distance of 50 km (Figure 1). The southwest side of MAT is Cocos Plate, which subducts beneath Caribbean Plate, on the northeast side of MAT, with the rate of 8~9 cm/yr [*Dixon*, 1993; *DeMets*, 2001]. However, the Cocos Plate contains tectonic and morphological boundary. Especially, two subducting oceanic crust plates, Cocos-Nazca Spreading center (CNS) beneath the southern Nicoya and East Pacific Rise (EPR) beneath the northern Nicoya, exist and are characterized with different geological age, topography, movement orientation, and heat flow distribution. The boundary is almost perpendicular to the MAT and cut through the central Nicoya Peninsula [*Barkhausen et al.*, 2001]. CNS has the age of 15~16 Ma, while EPS with the age of 22~24 Ma, which is relatively older than CNS [*Barkhausen et al.*, 2001]. CNS has relatively rough bathymetry, which is characterized with subducted seamounts [*Barkhausen et al.*, 2001, *Husen et al.*, 2003]; while EPR is dominated by smoother bathymetry [*Von Huene et al.*, 1995; *Protti et al.*, 1995a]. EPR crust subducts towards Nicoya parallel to the MAT. However, CNS crust subducts almost perpendicular to the trench [*Barkhausen et al*., 2001]. The heat flow measurements of CNS is about 110~120 $mW/m^2$, while the northern EPR crust is only 10-40 $mW/m^2$ [*Vacquier et al*., 1967; *Langseth and Silver*, 1996; *Fisher et al.*, 2001]. This thermal distribution was also proved by *Newman et al.* [2002] with illustrating that the up-dip limit of seismogenic zone of cooler EPR crust was 10 km deeper than that of warmer CNS crust. In

addition, *Spinelli et al*., [2006] detected that temperature variation at the boundary of these two oceanic crust results in the change of fluid pressure. Specifically, cooler EPR crust along the decollement is characterized with relatively higher fluid pressure. Seismic reflection and refraction study on the Nicoya region suggests a shallow angle of 6° of the slab interface near the trench; Moreover, the angle increases to 35° by 40 km depth [*Christeson et al.,* 1999; *Sallares et al.*, 1999, 2001] before reaching to 80° down-dip of the seismogenic zone [*Protti et al*., 1995b].

**Seismicity rate and interface locking**

**1. Introduction**

Grasping the knowledge of reoccurrence frequency of earthquakes, especially large earthquakes, has been being considered as one of the most significant and challenging questions in earthquake science. However, Gutenberg-Richter relation [*Gutenberg-Richter*, 1944; *Ishimoto and Iida*, 1939] can scientifically describe the relationship between the number of earthquakes with certain magnitude and the magnitude of earthquakes. The equation of this prevalent theory can be expressed by

$$lgN = a - bM$$

where *N* is the cumulative number of events greater than or equal to magnitude *M*, and *a* and *b* are constants [*Gutenberg-Richter*, 1944; *Ishimoto and Iida*, 1939]. Hence, the slope of this relationship, *b*-value, can reflect the ratio of small to large earthquakes. The worldwide average *b*-value is about 1 [e.g., *Stein and Wysession*, 2003].

Some scientists have been proposing that the *b*-value reflects the stress regime along the body or fault since 1960s. For instance, *Scholz* [1968] performed experiment by using different rock materials and applying different stress in the

laboratory, and the results showed that higher stress applied on the rock creates lower *b*-value. Furthermore, several other lab experiments also have been conducted to understand the physical meaning of *b*-value [e.g. *Warren and Latham*, 1970; *Wyss*, 1973; *Rabinovitch et al*., 2001, etc.]. On the other side, *Schorlemmer et al.*, [2005] also collected global earthquake catalog from different fault regimes, such as normal, strike-slip and thrust faults. They found out that *b*-values are highest near normal fault and that thrust faults tend to have the lowest values. Moreover, based on these results obtained from the global catalog, they also postulated that *b*-value can be utilized as an indicator of differential stress.

Especially, *Wiemer and Benoit* [1996] applied the mapping of frequency-magnitude distribution (FMD) in depth within Alaska and New Zealand subduction zones. They interpreted that high *b*-value region on the slab profile is associated with the high pore pressure for the reason of magmagenesis, which induces lower effective stress. Whereas *Sobesiak et al.,* [2007] and *Ghosh et al.,* [2008] made FMD mapping near subduction zones that are not associated with arc volcanism. Specifically, *Ghosh et al.* interpreted the low *b*-value region within Costa Rica subduction megathrust during interseismic period is associated with the increased interface locking, which was modeled by *Norabuena et al* [2004]. However, *Sobesiak et al.,* [2007] correlated high *b*-value region and positive gravity isostatic residual (IR) field after the *Mw*=8.0 Antofagasta earthquake near the subduction zone in Northern Chile. They interpreted the increased IR as an enhancement of local and regional mass distribution. Because the uplifted batholith structure beneath the continental crust is intruded by subducting oceanic plate after the main shock. It appears that these authors obtained an opposite results compared with previous research on *b*-values. In my opinion, the swarm of

aftershocks with relatively small magnitudes after the main events may increase the slope of seismicity numbers and magnitude.

Nonetheless, we cannot ignore the activities of tremor and slow slip events around the active tectonic environment of megathrust region. Conceptually, recorded tremor signal is semi-analogous and 'noise-like' earthquake signal, in which low-frequency (1-15 Hz) energy is more weighted than high-frequency energy [*Gomberg,* 2010, *Peng and Gomberg,* 2010]. Tremor is usually discovered near the subduction zone, and the occurrence of tremor is usually detected around the transitional regions between seismogenic zone and stable sliding zone [*Gomberg* 2010, *Peng and Gomberg*, 2010]. Scientists regard that the occurrence of tremor is usually associated with high fluid pressure [e.g*., Shelly et al*., 2006; *Brown et al*, 2009] along the fault. Meanwhile, scientists also have discovered that ground surface continuously and silently moves towards certain direction that is opposite to the original movement without being detected by seismometers in certain areas. These movements are termed as Slow Slip Events (SSE). Usually, the cumulative moment of this aseismic event is orders of magnitude larger than that of the common fast seismic events [*Peng and Gomberg* 2010]. *Outerbridge et al.,* [2010] detected slow-slip event accompanied by seismic tremor in 2007 near Nicoya Peninsula. In addition, *Walter et al.,* [2010] used a spectral method to locate tremor (2006-2009) around the Nicoya peninsula. Hence, it is possible that these aseismic events could be related to the local earthquakes. To certain extent, seismicity rate with different magnitude may also be affected by these tremor and slip events. The result may be reflected through the *b*-value map.

## 2. Data, Methodology and current result

## 2.1 Data Source and Processing

In order to systematically study the megathrust of Costa Rica, the Costa Rica Seismogenic Zone Project (CRSEIZE) was established by University of California, Santa Cruz, Observatorio Vulcanológico y Sismológico de Costa Rica, University of Miami, and University of California, San Diego. This project ran 10 on-land broadband seismometers and 4 short-period seismometers (Figure 2) in Nicoya Peninsula in 2009. The completeness of earthquake catalog has impact on the result of FMD study. Fortunately, Nicoya Peninsula is close to the MAT and the initial angle of downgoing plate is shallow, therefore the seismometers installed on the Peninsula can capture earthquake activity as much as possible [*Newman et al.*, 2002; *DeShon and Schwartz*, 2004; *Norabuena et al*., 2004; *DeShon et al.*, 2006]. Hence, we can take advantage of the abundant seismicity data.

Seismic waveform data are compiled and managed by using Antelope Relational Database System (Version 4.11) (Figure 3), which is developed by Boulder Real Time Technologies, Inc. (http://www.brtt.com). This program enables professional users of earthquake science manage and view the seismic waveforms. In addition, it also facilitates users to automatically or manually pick earthquakes by identifying the *P*- and *S*- wave arrivals, locate the hypocenters of seismic events, calculate the magnitudes, filter seismogram with different frequencies and perform other useful functions. In this study, the database of waveform from March 2009 to July 2009 were recorded and stored in the Antelope database. Here, I define this catalog as CR2009.

In order to verify the reliability of calculated local magnitudes from CR2009, which are determined by the algorithm of Antelope, I compare the CR2009 magnitudes with the magnitudes from ANSS (Advanced National Seismic System)

catalog. Furthermore, I also request for the catalog from Observatorio Vulcanológico y Sismológico de Costa Rica, OVSICORI, so that I could make another comparison of magnitudes. Because the catalog from ANSS is world wide, I only download the catalog of events with magnitude larger than 3, which is a relatively large magnitude in CR2009. The comparison (Figure 4, left) among 12 sparse events shows that the slope of fitting line is about 0.477+/-0.2959. Considering the sparse data and the magnitudes from ANSS are mostly moment magnitudes, which are usually higher than local magnitude, the magnitudes from CR2009 may still be reasonable. Furthermore, the comparison of magnitudes from CR2009 and OVSICORI (Figure 4, right) shows that the fitting slope is about 0.69+/-0.09. Here, local magnitudes are both used in these two different catalogs. Hence, the result indicates that the local magnitudes from catalog CR2009 are reliable.

In this research, I manually pick approximate 5500 events by identifying the *P*- and *S*- wave arrival times in Antelope 4.11. After the first location by using the integrated algorithm of Antelope, 1-D IASP91 velocity model, the location of the recorded events are relocated by using the 3-D velocity model of $V_p$ and $V_p/V_s$, which was derived by *DeShon et al* [2006]. This process is fulfilled by running a FORTRAN program -- *SIMULPS*12 [*Thurber*, 1983]. Because of the inadequate phase picking and the spatial limitation of *DeShon*'s velocity model [*Ghosh et al.*, 2008], 500 local events were removed from the catalog after running *SIMUPLS*12. In order to guarantee the accuracy of the event location, I also remove the earthquakes (~1500) with location error higher than 5km. Finally, 3445 earthquakes are kept in the catalog. In this study, I focus on the Nicoya Peninsula region and intend to verify the FMD pattern around the interface between downgoing Cocos plate and the Caribbean Plate. Hence, I demarcate horizontal boundaries by using the following geodetic coordinates:

(-86.5°, 11°), (-84.5°, 11°), (-86.5°, 8.5°) and (-84.5°, 8.5°). Then, I define two parabolic boundaries of this slab by fitting the microseismicities occurred along the plate interface, and remove the events with depth larger than 70 km. The purpose of demarcating the depth boundary is because earthquakes that are not close to the slab may not be involved with the seismogenic activity of the interface. In addition, earthquakes go beyond the downdip of seismogenic zone may have different mechanism of formation than those are within the seismogenic zone. Hence, 70km in depth, where subducting plate starts to stably slide without locking [*Norabuena et al.*, 2004], is selected as the end line. There is a coordinate transformation from geodetic coordinate to local Cartesian coordinate when creating the parabolic boundaries, so that I can visually check how these seismicities distribute relatively to the trench and constrain them into a 3-D range. I define (-85.5°, 9°) as the origin of this coordinate, and set a Y-axis that is approximately parallel to the trench, and set an X-axis that is perpendicular to Y-axis and pointing to the northeast direction. Here, Z-axis is orthogonal to the XY plane and pointing to the earth interior. And the two boundary curves are

$$y = -0.01(x - 30)^2 - 10$$

$$y = -0.009(x - 40)^2 + 15$$ (Figure 5).

Eventually, I use the well-located 1399 events to investigate the FMD along the megathrust interface.

**2.2 Methodology**

After gaining the reliable catalog, I input the subset catalog of 1399 events into a matlab program named *bval*, which is developed by *Ghosh et al*., [2008]. This program can be used to make grids on the region that are interested, search

earthquakes nearby each grid node by setting the number of events that are involved into the *b*-value determination, calculate *a*- and *b*- values, completeness magnitude, and relevant errors by using least square regression (LSR) and maximum likelihood estimation (MLE) [*Aki*, 1965; *Utsu*, 1965].

Here, least square fit method is a simple mathematical method. It only determines the fitting line by getting the minimum summation values of squared differences between the estimated line and individual points [*Scheaffer and McClave*, 1986]. On the other hand, MLE determines the slope of magnitude versus cumulative number of events by equation

$$b = log_{10} e/(\bar{M} - M_c)$$

where $\bar{M}$ is the mean magnitude, and $M_c$ is the completeness magnitude, below which the magnitude is excluded from the calculation of *b*-value. Hence, the determination of $M_c$ for MLE is the key to influence the deviation of *b*-value. *bval* uses maximum curvature method (MCM) [*Wiemer and Katsumata*, 1999; *Wiemer and McNutt*, 1997; *Wiemer and Wyss*, 2000], which takes the highest point of the curvature of the non-cumulative FMD as initial $M_c$. Then, *bval* uses this $M_c$ to determine a new $M_c$ for getting minimum misfit between discrete data and synthetic line [*Wiemer and Wyss*, 2000].

I set 0.025°× 0.025° as the horizontal unit grid to map the FMD. In order to obtain an optimal number of sampling events for each grid, I test the variation (Figure 6) of *b*-values and sampling radius for grid nodes 1, 2 and 3 in figure 2 when the sampling events change. In figure 6.c, *b*-value is not so stable before counting 130 events to perform the seismicity rate determination when testing node locates where less earthquakes occurred. However, *b*-values are all relatively stable near 150 sampling events in this test. Besides, the sampling radius doesn't exceed 30 km for these 3

nodes when sampling number is around 150. In particular, large sampling area may induce inaccurate reflection of local *b*-value for each grid. Even though increasing sampling radius may produce relatively stable *b*-value curve, I still set 150 as the number of events that are searched nearby each grid node in the catalog to calculate *b*-values. In addition, I use 60km as the longest sampling radius in this case. After finishing these settings and running *bval*, each grid will have *b*- value, $M_c$, error of *b*-value, etc. These parameters are illustrated in colors in figure 10, 11 and 12.

**2.3 Results and discussion**

The overall *b*-value (Figure 8) for the subset catalog is 0.94+/-0.039 by using MLE. Meanwhile, LSR method deduces that the overall b-value (Figure 9) is 0.91+/-0.03. These two results are pretty close to the global average *b*-value [e.g. *Stein and Wysession*, 2003], which is 1. However, they are still higher than the published subduction zone *b*-value, which is between 0.5 and 0.8 [*Bayrak et al*., 2002]. This result is consistent with the FMD that was calculated by using the seismic catalog (Nicoya1999) between late-1999 and mid-2001 within the same region [*Ghosh et al*., 2008]. The spatial distribution of seismicity rate varies from 0.5 to 2.4. The MLE results of *b*-value for grid nodes 1, 2 and 3 by using the subset catalogs of nearby 150 events are shown in figure 9. Here, maps of *b*-values that are calculated by MLE and LSR (Figure 10 left and 11 left) share the similar pattern, even though there are specific differences on the FMD. It is obvious that northwest side of Nicoya Peninsula is characterized with relatively low *b*-values. On the other hand, the southeast region of Nicoya Peninsula is covered with relatively high *b*-values. The errors of *b*-value in figure 10 (right) are also determined by LSR method. However, Bootstrapping statistical method is applied in the process of calculating *b*-value errors by using MLE.

For each grid node, bootstrap of random selecting earthquakes creates 10000 subset catalogs, and the errors of *b*-values (Figure 11 right) are determined by the *b*-values calculated from these 10000 catalogs. The process of random sampling in the same subset catalog makes the error results more reliable and stable. Furthermore, the result indicates that errors of *b*-values are less than 0.5 in the interested region. The distribution of $M_c$ that is determined by MLE for each grid node is displayed in figure 12.

In order to verify whether the fitting parabolic boundaries of slab have the function of eliminating influence of earthquakes that may have different mechanism, I also make two separated FMD maps by using LSR and MLE methods respectively, and the whole catalog without setting any boundary. The results are shown in figure 13 and 14. Comparing figure 10 and 11 with figure 13 and 14 respectively, it is obvious that the *b*-values of inland portion in this area have been increased after eliminating the fitting boundaries of slab. In my interpretation, swarms of events with relatively smaller magnitude occurred in the shallow continental crust cause the slope of ratio between number of smaller and larger events increased. The relevant errors of *b*-values are also shown in figure 13 and 14. Hence, it is undeniable that setting the slab boundaries plays its role in excluding the negative influence of other events that may have different occurrence mechanism.

However, the patches of high and low *b*-values (Figure 15) in 2009 calculated by MLE are somehow different from the previous FMD map (Figure 16) that is produced by MLE and the Nicoya1999 catalog. The major difference between them is the northwest region with *b*-values of 2.0 has become the low-*b* region. In this new dataset, I only obtain *b*-value around 0.7 on the northwest corner of Nicoya. There are a couple of reasons to cause this variation: 1). The reliability of this catalog should be

considered. The slope of fitting line (Figure 4) produced by magnitudes from CR2009 versus magnitudes from ANSS and VOSICORI are relatively small. This indicates that the number of smaller events might be underestimated, so that the *b*-values might be increased after using CR2009 catalog. However, my results do not reflect this phenomenon; ironically, *b*-values decrease after all. Hence, the possible system errors from our catalog are not the reason for creating this difference. 2). The characteristics of interface near EPR have been changed after ten years. Because Nicoya Peninsula is still experiencing the interseismic period of large earthquakes (magnitude > 7.5), which have been occurring every 50 years (1853, 1900 and 1950 [*Brown et al*., 2006]). It is possible that the locking portion [*Norabuena et al*., 2004; *Ghosh et al*., 2008], which located near the offshore region of Nicoya at the boundary of EPR and CNS, has migrated to the northwest side of the peninsula. If this is the case, the obvious boundary of low and high *b*-value regions near the offshore of Nicoya shares the similar boundary of EPR and CNS. 3) Other tectonic phenomena may be interrupting the evolution of subduction interface locking. Tremor occurred from 2006 to 2009 has been continuously detected near the Costa Rica subduction megathrust [*Walter et al*., 2010]. Coincidently, the locations of tremor occurred near Nicoya in April 2009 were distributed along the northwest coast of Nicoya. Moreover, major tremor episode happened around this region in April 2009. By plotting the histogram of earthquakes (Figure 17) within the parabolic slab from CR2009, a sudden increase of daily earthquake number also occurred in the middle of April 2009. In order to verify if the April major tremor episode affects the low *b*-values, events in April are excluded from the catalog. 1020 events are used to make another FMD map for comparison. Considering the inadequate data after removing 359 events, I set the number of subset catalog for each grid node is 100. However, the grid spacing is still 0.025° × 0.025°.

Specifically, I use MLE method to create the seismicity rate distribution map. Because this method determines the slope of seismicity number versus magnitude by mean magnitude and completeness magnitude, *b*-value will be relatively stable without being influenced by large magnitude events, which are rarely because of inadequate time period. Surprisingly, the results of FMD (Figure 18), which excludes the events in April 2009, have similar pattern with the one includes events in April 2009 (Figure 15). At least, the outcome indicates that the major tremor episode in April 2009 did not affect the seismicity rate. It also indicates that the tremor episode did not change the accumulated stress on the subducting plate interface.

The maximum slip area of slow slip event occurred in 2007 [*Outerbridge et al., 2010*] is coincident with the high *b*-value region (Figure 15). In my opinion, slow slip events that occurred in the southeast part of Nicoya have released most of the accumulative stress on the subducting interface. In this way, the earthquakes within this region occurred after 2007, which follow the stick-slip fashion, are not supposed to be big in magnitude. Therefore, larger proportion of seismic events with smaller magnitudes increases the *b*-values which are reflected on the FMD map. In addition, another unpublished geodetic study in the same area [*Feng et al., 2010 AGU talk*], which uses GPS deformation data collected between 1996 and 2010, also supports my interpretation. One fully locked portion (Figure 15) determined by geodetic inversion covers the central Nicoya Peninsula where is characterized with low *b*-values. However, the other locked patch near the southeast offshore region doesn't coincide with low *b*-values in my FMD map. There are a couple of reasons to explain the difference: 1) my results are determined by the ratio of occurrence of small earthquakes to large ones. However, the time span of our catalog only covers less than 5 months. It is really difficult to expect many earthquakes with large magnitude (e.g,

local magnitude > 5) occur within such short period of time. Hence, low *b*-value region may not be unveiled by using our catalog; 2) the geodetically derived interface coupling use GPS data that spans more than 10 years. However, this model does not consider the slow slip events occurred in May 2007 [*Outerbridge et al.* 2010], August 2008 and 2009 [*Walter et al.,* 2011]. Common sense tells us that the reversed movement of these slip events, which move with the rate of 12 cm in approximate 40 days [*Outerbridge et al., 2010*], may have some influence on the locking pattern along the plate interface. The results from geodetic model may need further study.

Compared with the spatial FMD map by using catalog from late 1999 to mid-2001 within Nicoya region, newly generated FMD map have even wider area with low *b*-values (~0.8) along the central and northwest coastline of Nicoya. This may reflect that the stress distribution around this region has been changed.

**Seismogenic interface locking determined by geodetic method**

**1. Previous work**

In order to study the seismic cycle and plate deformation near Costa Rica subduction zone, *Lundgren et al.* [1999] organized three GPS campaigns on 23 sites distributed in Costa Rica in 1994, 1996 and 1997. Most sites were occupied for 3-5 days, while some of them were up to 2 weeks. By testing the locked segment of downgoing plate through applying dislocation model of *Okada* [1985], the authors estimated that the fault from 70 to 95 km away from the trench is locked. In addition, they established the inversion model to produce the fault slip rate by assuming that the downgoing interface is composed of seven continuous planes with variable depths and dip angles. Eventually, they extrapolated that central and southeast portion of Nicoya is highly locked.

*Norabuena et al.* [2004] continued to collect GPS campaign data in this area in 2000 (3-5day observations at most sites from January to February 2000). Moreover, they set up more new monument and occupied in order to obtain abundant GPS data of ground movement for future research. *Norabuena et al.* [2004] improved the inversion model by considering both the elastic deformation and permanent deformation. In Nicoya, they estimated two ~60% locked patches at 14±2 and 39±6 km depth. When applying this model, they also defined the geometry of plate interface as three adjoining plane segments with different dips. In addition, they also estimated the northwest motion of fore-arc block with rate of 8±3mm/yr.

In particular, *Feng et al.* [2010, *AGU talk*] utilized old GPS campaign data of Nicoya in 1996, 2000 and 2003, plus the new GPS campaign data in 2010 to obtain the inversion fault slip. They estimated that fully locked (back slip ~8cm/yr) interface distribute mainly at the central Nicoya coastline, northwest and southeast offshore region of Nicoya. Compared with the results from *Norabuena et al.* [2004], the coupling degree has increased from approximately 60% to 100%. Furthermore, the locked patches also cover larger area from *Feng*'s results. Longer time span of GPS displacement data may give better resolution to the seismogenic interface coupling.

As what I have previously mentioned, *Outerbridge et al.* [2010] used the network of GPS and seismic stations on Nicoya to detect the Episodic Tremor and Slip (ETS) occurred near Nicoya in May 2007. By obtaining the inversion results of ground displacement data, they discovered the maximum slip happened at a depth of 25-30 km, where is near the downdip of seismogenic zone; on the other hand, they also estimated that another slip patch has reverse slip (~5 cm) at ~6 km depth, where is

close to the updip boundary of seismogenic zone. The fault geometry of three adjoining planes [*Norabuena et al.,* 2004] was still used in their study.

Many published papers have proved that the transition boundary does exist between the CNS and EPR oceanic crusts, such as age [*Barkhausen et al.*, 2001], temperature [*Vacquier et al*., 1967; *Langseth and Silver*, 1996; *Fisher et al.*, 2001], and fluid pressure difference [*Spinelli et al*., 2006]. Specifically, *Deshon et al*. [2006] also presented the 3-D seismic velocity model below Nicoya Peninsula and identified that plate interface have offset between EPR and CNS crust. Basically, the geometry of interface is the significant prerequisite for better understanding the tectonic process and, especially, the stress accumulation pattern. Usually, previous geodetic inversion models [e.g., *Lundgren et al.*, 1999; *Norabuena et al.*, 2004; *Outerbridge et al.*, 2010, etc.] built on this region just use the linear or non-linear 2D plate interface to solve the slip rate on the fault. However, my advisor Dr Newman and his former student have developed a 3-D interface [*Thomas et al*., 2007] by using the several Costa Rica local earthquake datasets and other teleseismic dataset (e.g., global CMT catalog, NEIC catalog, EHB catalog and etc.). They defined the interface by searching the maximum density of seismicity within approximate parabolic boundaries of the slab.

**2. Future work**

In order to verify the significance of this 3-D subducting interface beneath Nicoya, especially the transitional change of EPR and CNS crusts, I plan to utilize the data of four GPS campaigns on Nicoya (from 1996 to 2010) and apply this seismic interface model to solve for the fault slip. After that, I will verify if there is big change over the fault locking distribution compared with *Feng*'s [2010 AGU talk] results, so that we can identify the impact of 3-D interface on solving for the inversion slip and

accumulated shear stress on the fault. I will build up this model by using ABAQUS (www.abaqus.com) to perform the finite element model.

Because of the slow slip events occurred beneath Nicoya, the surface horizontal displacement recorded by continuous GPS stations exhibit the zigzag fashion. Previous studies on the geodetic methods of solving interface locking beneath Nicoya normally do not take into account the slow slip events. Usually, researchers treat the zigzag fashion of surface displacement as a flat line in the long term running. However, many slow slip events have been detected within Nicoya region. I plan to divide the continuous GPS dataset by the occurrences of SSE, and chuck out the data during SSE, so that I can use the separated dataset (no SSE occurred) within 2~3 years to obtain separated coupling distributions beneath Nicoya. By doing this, I can easily see how locking pattern changes before and after the SSE. Hence, I also can verify whether accumulated stress on the subduction fault can be influenced by this aseismic phenomenon. If it is possible, I may also apply the 3-D seismic interface model in this study of SSE influence on the interface coupling.

**Acknowledgements**

I thank for Dr Andrew Newman, Dr Zhigang Peng, Lujia, and Chunquan, Brendan, Chastity and Xiaofeng for the thoughtful advice, I also thank Victoria Van Cappellen for revising my abstract and giving advice on writing skill. Figures were developed using GMT and Matlab.

**References**


Aki, K. (1965), Maximum likelihood estimate of b in the formula log10 N = a - b M and its confidence limits, Bull. Earthquake Res. Inst. Univ. Tokyo, 43, 237–239.

A. Rabinovitch, et al (2001) Gutenberg-Richter-type relation for laboratory fracture-induced electromagnetic radiation, Physical review E, Volume 65,011401, DOI: 10.1103/PhysRevE.65.011401

Barckhausen, U., C. R. Ranero, R. von Huene, S. C. Cande, and H. A. Roeser, Revised tectonic boundaries in the Cocos plate off Costa Rica: Implications for the segmentation of the convergent margin and for plate tectonic models, *J. Geophys. Res., 106*, 19,207– 19,220, 2001.

Bayrak, Y., A. Yılmaztürk, and S. Öztürk, Lateral variation of the modal (a/b) values for the different regions of the world, *J. Geodyn., 34*, 653-666, 2002.

Brown, K., A. V. Newman, R. Stevens, K. McIntosh, N. Bangs, D. Chadwell, S. Bilek, G. Spinelli, S. Schwartz, L. Dorman, E. Silver, D. Hilton, M. Kastner, G. McMurty, and G. Wheat (2006), A plate boundary observatory at Costa Rica, *MARGINS Newsletter*, Spring 2006, *16*, 19-20 (cont. 37).

Brown, J. R. et al. Deep low-frequency earthquakes in tremor localize to the plate interface in multiple subduction zones. Geophys. Res. Lett. 36, L19306 (2009).

Christeson, G. L., K. D. McIntosh, T. H. Shipley, E. R. Flueh, and H. Goedde, Structure of the Costa Rica convergent margin, offshore Nicoya Peninsula, J. Geophys. Res., 104, 25,443–25,468, 1999.

DeMets, C., A new estimate for present-day Cocos-Caribbean plate motion: Implications for slip along the Central American volcanic arc, Geophys. Res. Lett., 28, 4043–4046, 2001.

DeShon, H. R., and Schwartz, S.Y., Evidence for Serpentinization of the Forearc mantle wedge along the Nicoya Peninsula, Costa Rica, *Geophys. Res. Lett.*, 31 (L21611), doi:10.1029/ 2004GL021179, 2004.

DeShon, H. R., S. Y. Schwartz, L. M. Dorman, A. V. Newman, V. Gonzalaz, M. Protti, T. Dixon, E. Norabuena & E. Flueh, Seismogenic zone structure along the Middle America Trench, Nicoya Peninsula, Costa Rica, from 3D local earthquake tomography using *P*- and *S*-wave data , *Geoph. Jrn. Int.*, 164 (1), 109-124, 2006.

Dixon, T. H., GPS measurements of relative motion of the Cocos and Caribbean plates and strain accumulation across the Middle America Trench, *Geophys. Res. Lett., 20*, 2167– 2170, 1993.

Fisher, A. T., et al., Heat flow on the incoming plate offshore Nicoya, Costa Rica margin: Implications for hydrothermal circulation and the thermal state of the subducting plate, Trans. Am. Geophys. Union (EOS), 82, F1150, 2001, [Abstract].

Ghosh, A., A. V. Newman, A.M. Thomas, G. T. Farmer, Interface locking along the subduction megathrust from microseismicity near Nicoya, Costa Rica, *Geoph. Res. Lett.*, 35, L01301, doi:10.1029/2007GL03161, 2008.

Gutenberg, B., and C. F. Richter (1944), Frequency of earthquakes in California, Bull. Seismol. Soc. Am., 34, 185–188.

Husen, S., R. Quintero, E. Kissling, and B. Hacker, Subduction-zone structure and magmatic processes beneath Costa Rica constrained by local earthquake tomography and petrological modeling, *Geophys. Journ. Int. 155* (1), 11–32. doi:10.1046/j.1365-246X.2003.01984, 2003.

Ishimoto, M., and K. Iida (1939), Observations of earthquakes registered with the microseismograph constructed recently, Bull. Earthquake Res. Inst. Univ. Tokyo, 17, 443–478.

Joan Gomberg, et al (2010), Slow-slip phenomena in Cascadia from 2007 and beyond: A review.GSA Bulletin; July/August 2010; v. 122; no. 7/8; p. 963–978; doi: 10.1130/B30287.1; 10 figures.

Langseth, M. G., and E. A. Silver, The Nicoya convergent margin; a region of exceptionally low heat flow, Geophys. Res. Lett., 23, 891–894, 1996.

Lundgren, P., M. Protti, A. Donnellan, M. Heflin, E. Hernandez, and D. Jefferson (1999), Seismic cycle and plate margin deformation in Costa Rica: GPS observations from 1994 to 1997, *J. Geophys. Res., 104(B12),* 28,915-28,926.

M. Dorman, E. Flueh, P. Lundgren, F. Pollitz, D. Sampson, Geodetic and seismic constraints on some seismogenic zone processes in Costa Rica, *J. Geophys. Res.*, 109 (B11403), doi:10.1029/2003JB002931, 2004.

Newman, A. V., S. Y. Schwartz, V. Gonzalez, H. R. DeShon, J. M. Protti, and L. M. Dorman, Along- strike variability in the seismogenic zone below Nicoya Peninsula, Costa Rica, Geophys. Res. Lett., 29(20), 1977, doi:10.1029/ 2002GL015409, 2002.

Norabuena, E., T. H. Dixon, S. Y. Schwartz, H. R. DeShon, A. V. Newman, M. Protti, V. Gonzalez, L.

Okada Y., Surface deformation due to shear and tensile faults in a half- space, Bull .Seismol. Soc, Am., 75,1135-1154, 1985.

Outerbridge, K. C. , T. H. Dixon, S. Y. Schwartz, J. I. Walter, M. Protti, V. Gonzalez, J. Biggers, M. Thorwart, and W. Rabbel (2010), A tremor and slip event on the Cocos-Caribbean subduction zone as measured by a global positioning system (GPS) and seismic network on the Nicoya Peninsula, Costa Rica, *J. Geophys, Res*., 115 B10408, doi: 10.1029/2009JB006845.

Pacheco, J. F., and L. R. Sykes, Seismic moment catalog of large, shallow earthquakes, 1900 – 1989, Bull. Seismol. Soc. Am., 82, 1306 – 1349, 1992.

Peng Zhigang and gomberg Joan (2010), An integrated perspective of the continuum between earthquakes and slow-slip phenomena. Nature Geoscience,| doi: 10.1038/ngeo940

Protti, M., F. Gundel, and K. McNally, Correlation between the age of the subducting Cocos plate and the geometry of the Wadati-Benioff zone under Nicaragua and Costa Rica, in Geologic and Tectonic Development of the Caribbean Plate Boundary in Southern Central America, edited by P. Mann, Spec. Pap. Geol. Soc. Am., 295, 309–326, 1995a.

Protti, M., et al., The March 25, 1990 (Mw = 7.0, ML = 6.8), earthquake at the entrance of the Nicoya Gulf, Costa Rica: Its prior activity, foreshocks, aftershocks, and triggered seismicity, J. Geophys. Res., 100, 20,345– 20,358, 1995b.

, E. R. Flueh, and G. Leandro, Seismic velocity structure across the middle American landbridge in northern Costa Rica, J. Geodyn., 27, 327–344, 1999.

, and E. R. Flueh, Lithospheric structure of the Costa Rican Isthmus: Effects of subduction zone magmatism on an oceanic plateau, J. Geophys. Res., 106, 621 – 643, 2001.

Scheaffer, R. L., and J. T. McClave (1986), *Probability and Statistics for Engineeres*, Duxbury Press, Boston.

Scholz, C. H. (1968), The frequency-magnitude relation of microfracturing in rock and its relation to earthquakes, Bull. Seismol. Soc. Am., 58, 399 – 415.

Schorlemmer, D., S. Wiemer, and M. Wyss (2005), Variation in earthquake- size distribution across different stress regimes, Nature, 437, 539–542, doi:10.1038/nature04094.

Sobiesiak, M., U. Meyer, S. Schmidt, H.-J. Götze, and C. M. Krawczyk, Asperity generating upper crustal sources revealed by *b* value and isostatic residual anomaly grids in the area of Antofagasta, Chile, *J. Geophys. Res.*, 112, B12308, doi:10.1029/2006JB004796, 2007.

Shelly, D. R., Beroza, G. C. & Ide, S. Low-frequency earthquakes in Shikoku, Japan, and their relationship to episodic tremor and slip. Nature 442, 188–191 (2006).

Spinelli, G., D. Saffer, and M. Underwood, Hydrogeologic responses to three-dimensional temperature variability, Costa Rica subduction margin, *J. Geophys. Res.*, *111*, doi:10.1029/2004JB003436, 2006.

Stein, S., and M. Wysession (2003), An Introduction to Seismology, Earth- quakes, and Earth Structure, Blackwell, Oxford, U. K.

Thomas, A. M., A. V. Newman, A. Ghosh and G. T. Farmer, Statistical Modeling of the Middle America Subduction Zone Using Interplate Seismicity, *Seismo. Res. Let. , Ann. Meet. Suppl*., [abstract] 2007.

Thurber, C. H., Earthquake locations and three-dimensional crustal structure in the Coyote Lake area, central California, *J. Geophys. Res.*, **88**, 8226−8236, 1983.

Utsu, T. (1965). A method for determining the value of b in a formula log n = a - bM showing the magnitude frequency for earthquakes, *Geophys. Bull. Hokkaido Univ.* **13,** 99–103.

Vacquier, V., J. Sclater, and C. Corry, Studies in the thermal state of the earth, the 21st paper: heat-flow, eastern pacific, Bull. Earthqu. Res. Inst., 45, 375–439, 1967.

Von Huene, R., et al., Morphotectonics of the Pacific convergent margin of Costa Rica, in Geologic and Tectonic Development of the Caribbean Plate Boundary in Southern Central America, edited by P. Mann, Spec. Pap. Geol. Soc. Am., 295, 291–307, 1995.

Walter, J. I., S. Y. Schwartz, J. M. Protti, and V. Gonzalez(2011), Persistent tremor within the northern Costa Rica seismogenic zone, *Geophys, Res. Lett.*, 38, L01307, doi:10.1029/2010GL045586.

Warren, N. W., and G. Latham (1970), An experiment study of thermal induced micro-fracturing and its relation to volcanic seismicity, J. Geo- phys. Res., 75, 4455–4464.

Wiemer, S., and J. P. Benoit (1996), Mapping the b-value anomaly at 100 km depth in the Alaska and New Zealand subduction zones, *Geophys. Res. Lett., 23(13)*, 1557-1560.

Wiemer, S., and K. Katsumata (1999), Spatial variability of seismicity parameters in aftershock zones, *J. Geophys. Res., 103,* 13,135–13,151.

Wiemer, S., and M. Wyss (2000), Minimum magnitude of completeness in earthquake catalogues: Examples from Alaska, the western United States, and Japan, Bull. Seismol. Soc. Am., 90, 859–869.

Wiemer, S., and S. R. McNutt (1997), Variation in the frequency-magnitude distribution with depth in two volcanic areas: Mount St. Helens, Washington, and Mt. Spurr, Alaska, *Geophys. Res. Lett., 24(2)*, 189-192.

Wyss, M. (1973), Towards a physical understanding of the earthquake frequency distribution, Geophys. J. R. Astron. Soc., 31, 341–359.

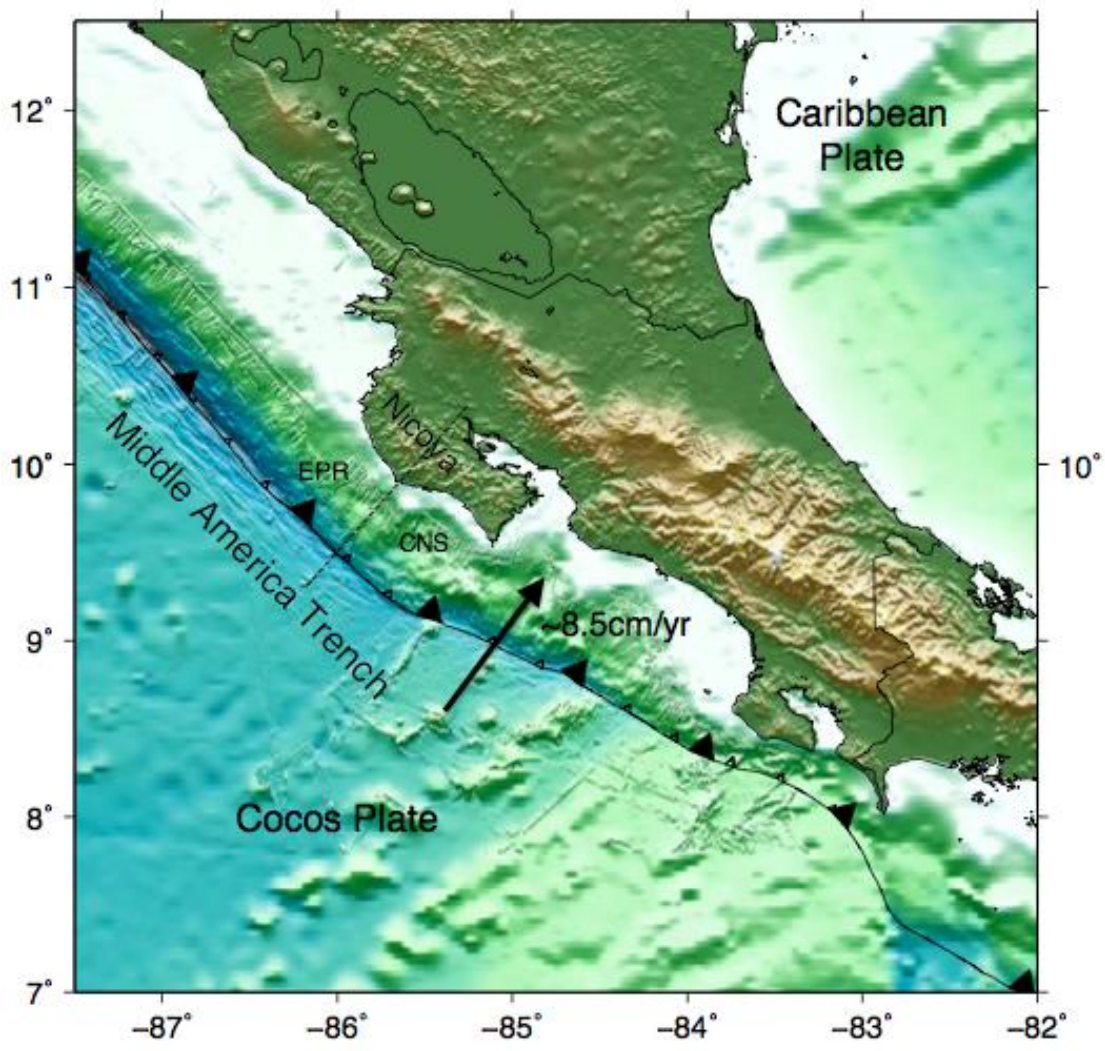


Figure 1. Coco's Plate subducts beneath the Caribbean plate with the convergence rate of ~8.5 cm/yr near the central America area.[*DeMets*, 2001]. Saw-toothed curves is the Middle America Trench. Transitional boundary exists between EPR and CNS oceanic plates near Nicoya Peninsula, Costa Rica.

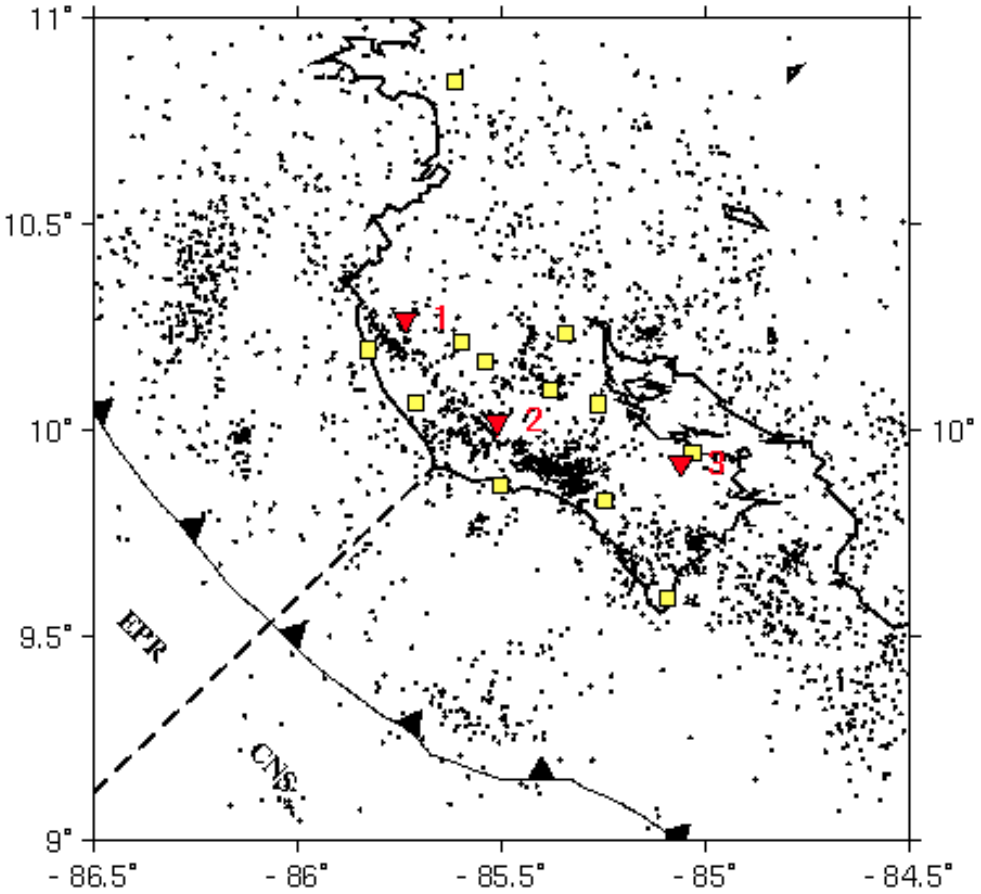


Figure 2. 10 on-land broadband seismometers and 4 short-period seismometers, which are represented by yellow squares, are distributed on Nicoya Peninsula. Black dots are earthquakes (horizontal location error less than 5km). Dash line is the transitional boundary between EPR and CNS. Saw-soothed curve is the Middle America Trench. Red triangles with numbers on their right side are the locations that I will use for specific discussion in the following sections.

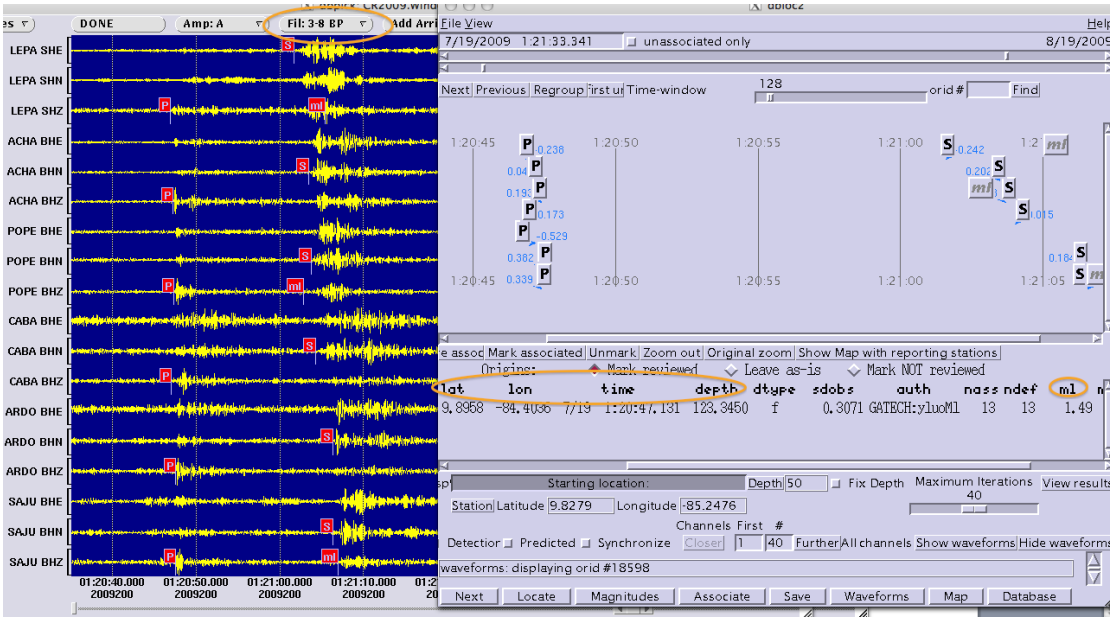


Figure 3. Interface of Antelope (4.11). 3-8Hz broadband filter is applied on the seismogram. By manually picking the P- and S- wave arrival phase, the occurrence time, location and local magnitude of specific earthquake are determined by the integrated algorithm of Antelope.

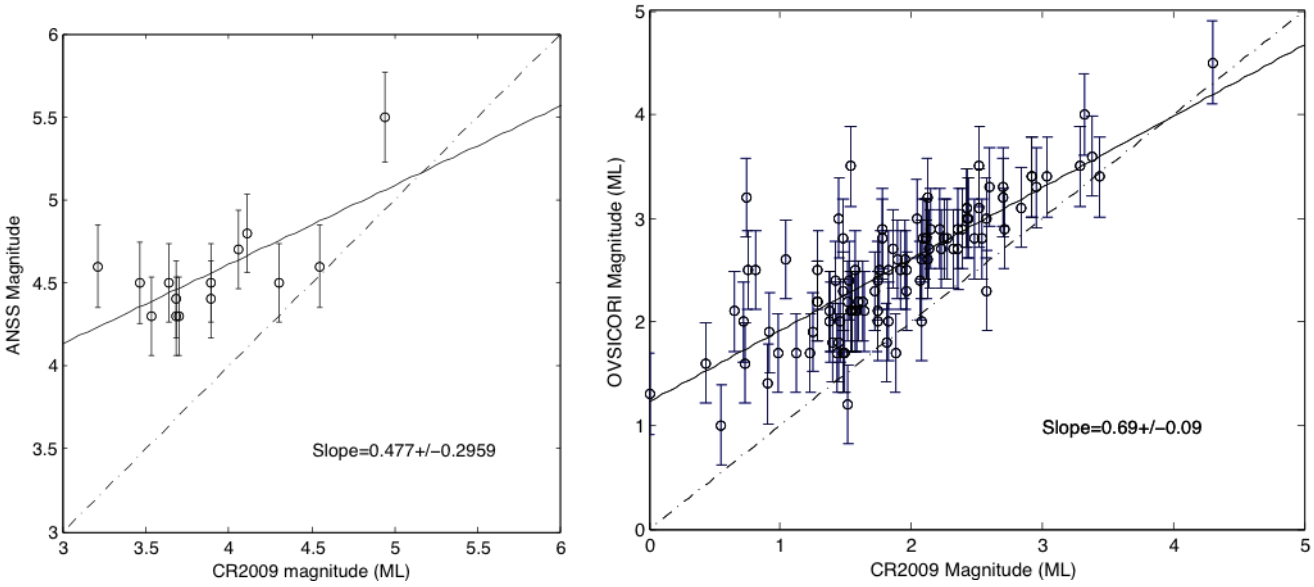


Figure 4. (Left) comparison between the local magnitude of CR2009 and magnitude of ANSS (most of them are moment magnitude). Solid line is the best-fit line with slope of 0.477; (right) comparison between the local magnitude of CR2009 and local

magnitude of OVSICORI. The best-fit line has a slope of 0.69. Dashed lines represent the slope of 1.

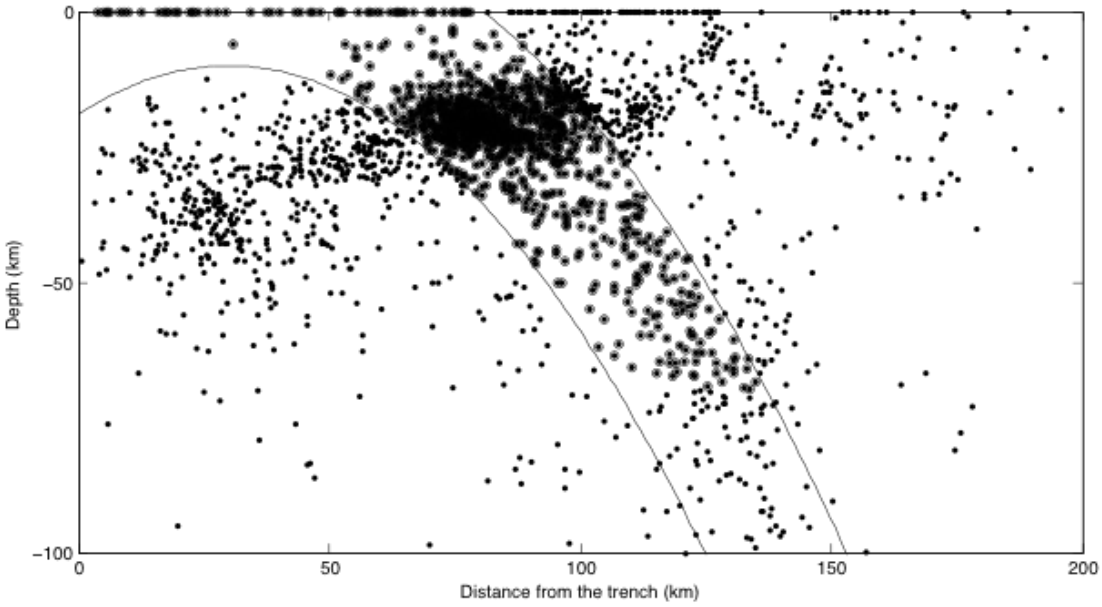


Figure 5. Cross-section view of seismicity. Circles with center represent earthquakes (depth < 70km) occurred within the parabolic boundaries of subducting slab, and these earthquakes are used for this study. Smaller dots are earthquakes that have been excluded from the catalog.

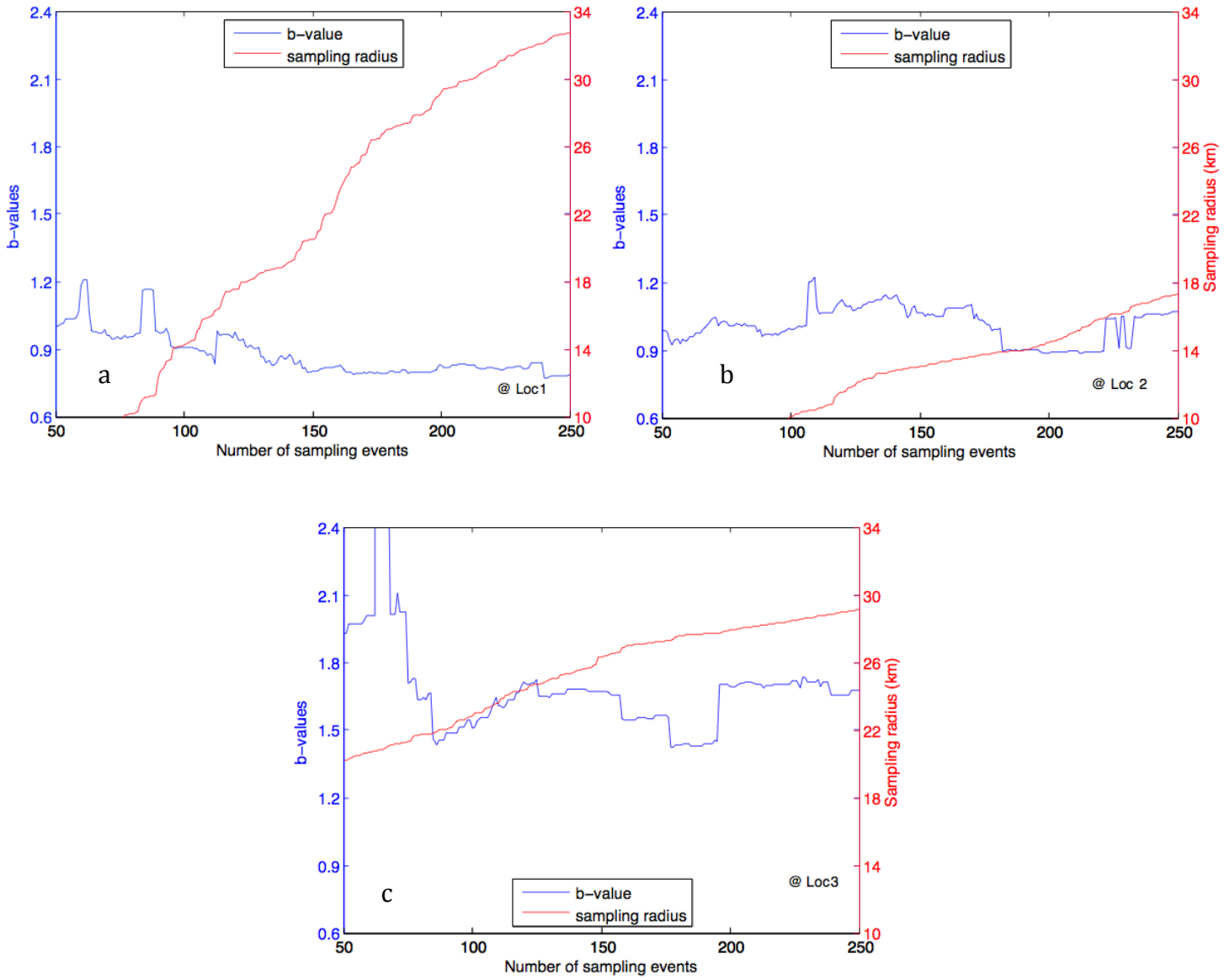


Figure 6. Variation of *b*-values and sampling radius when changing the numbers of sampling events at location 1, 2, and 3 in figure 2.

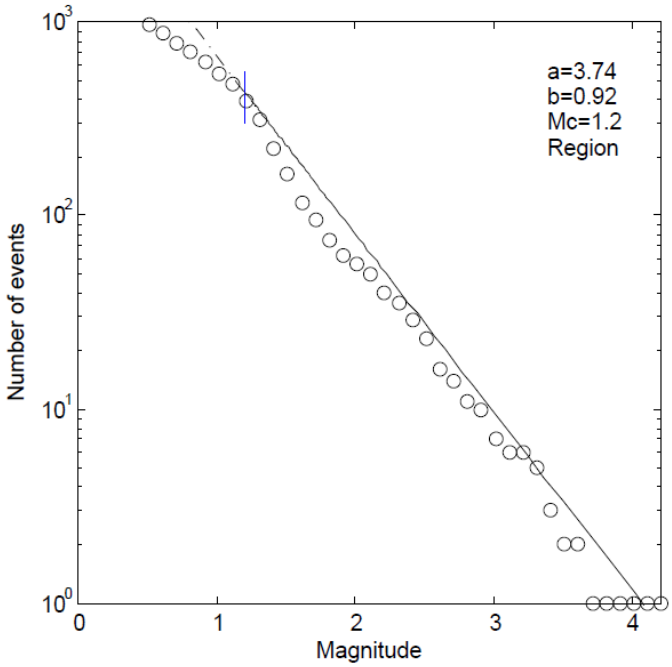


Figure 7. Overall *b*-value of the events within slab. The *b*-value is determined by using LSQ method. Circles represent cumulative numbers of event. Blue vertical line shows the completeness magnitude.

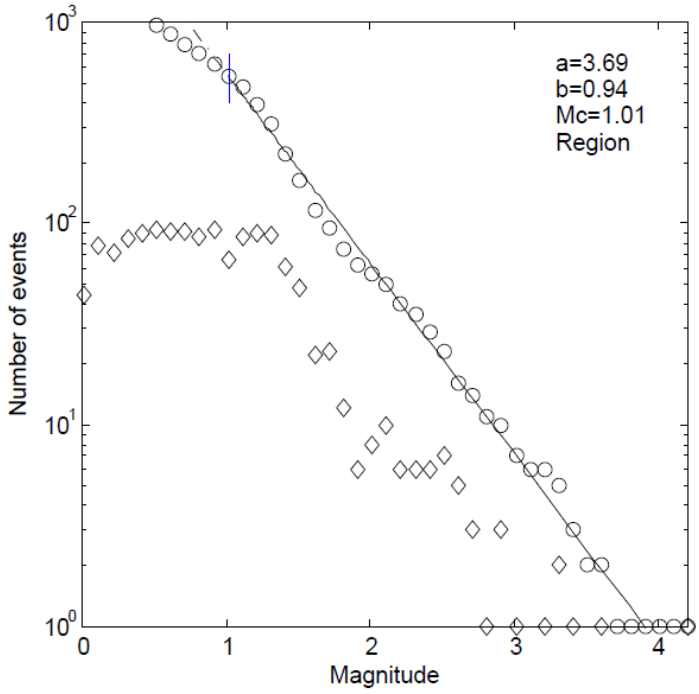


Figure 8. Overall *b*-value of the events within slab. The *b*-value is determined by using MLE method. Circles represent cumulative numbers of events. Diamonds

represent non-cumulative numbers of events. Blue vertical line shows the completeness magnitude.

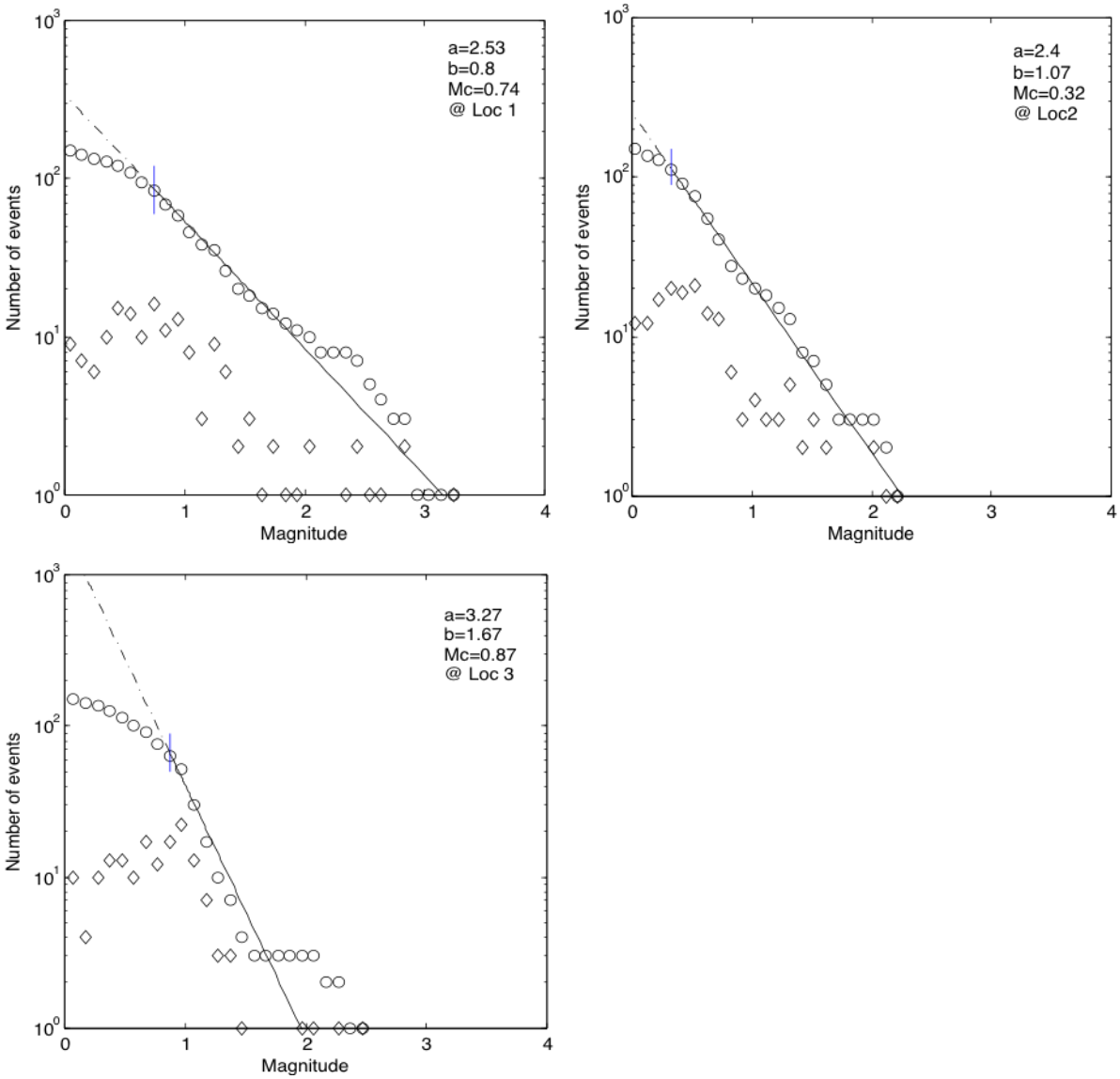


Figure 9. *b*-values of subset catalog for grid node 1, 2 and 3 in figure 2. Circles represent cumulative numbers of events. Diamonds represent non-cumulative numbers of events. Blue vertical lines show the completeness magnitude.

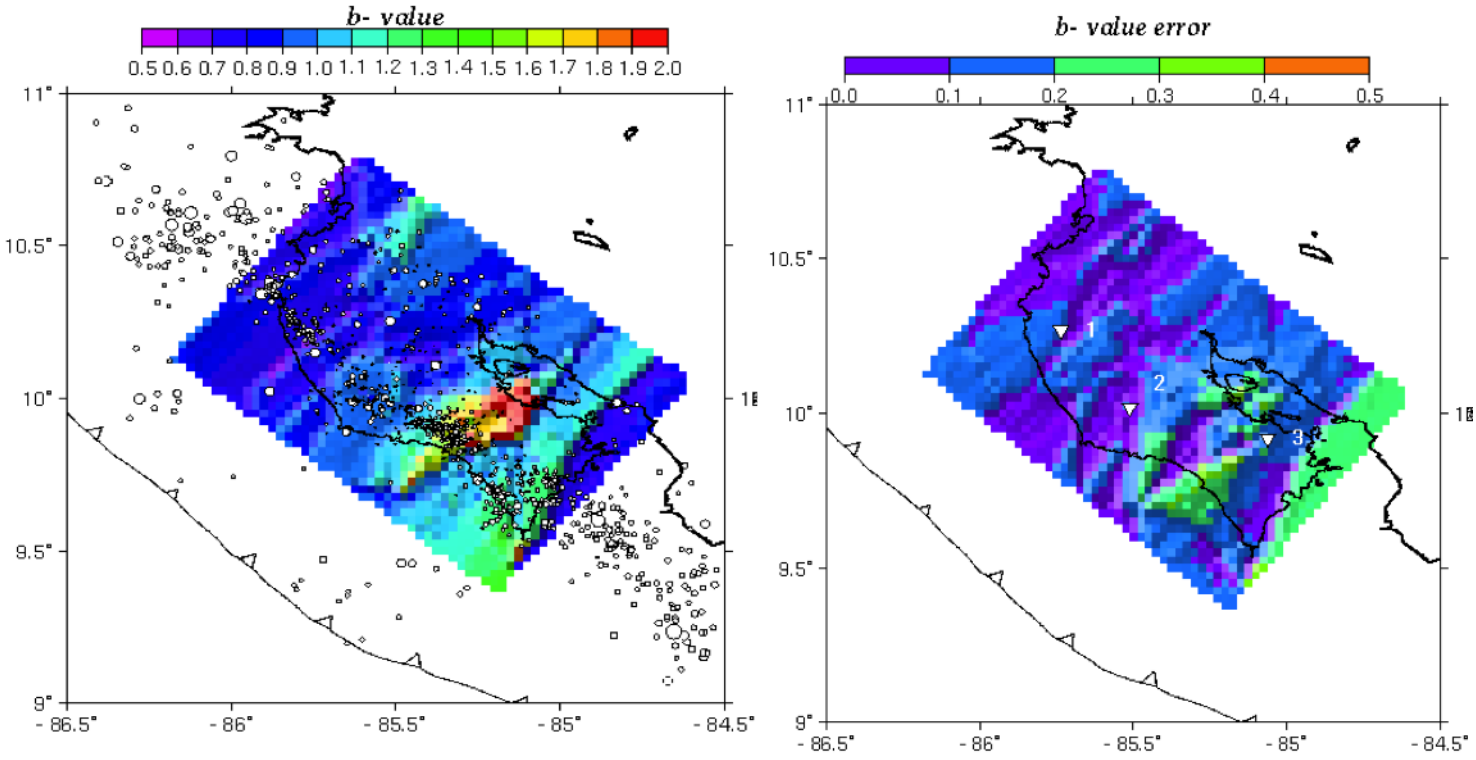


Figure 10. (Left)Spatial distribution of *b*-values by using least square regression method and catalog of events within the fitting slab. Open circles represent earthquakes within the slab. (Right) Relevant errors of *b*-value determined by least square regression. Triangles are grid nodes used in figure 9

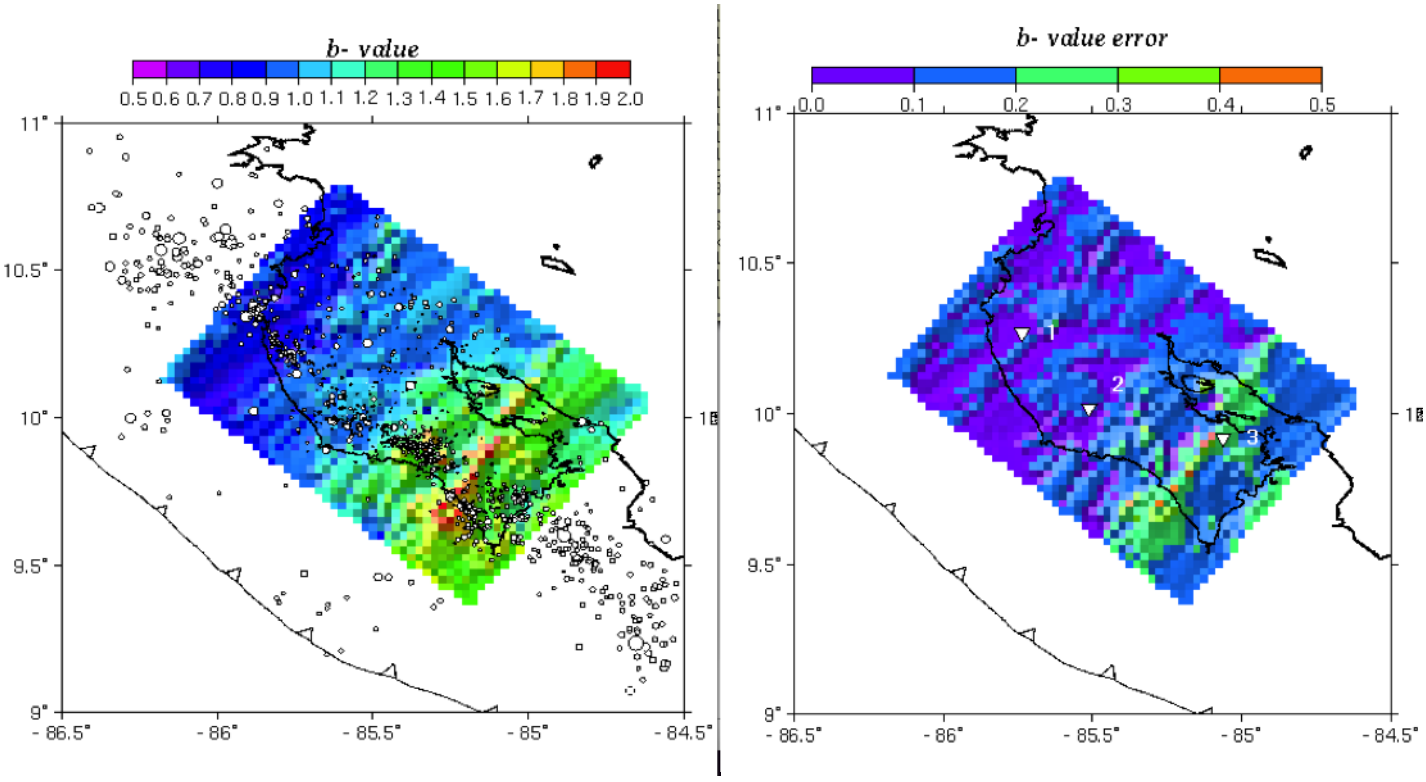

Figure 11. (Left) Spatial distribution of *b*-values by using maximum likelihood estimation method and catalog of events within the fitting slab. Open circles represent earthquakes within the slab. (Right) Relevant errors of *b*-value determined by bootstrap method. Triangles are grid nodes used in figure 9

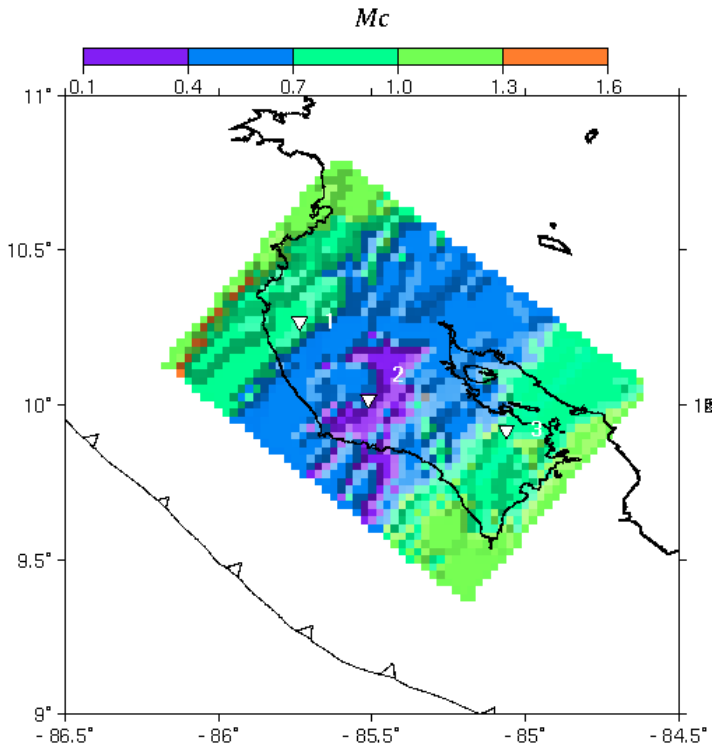


Figure 12. Spatial distribution of completeness magnitude by using maximum curvature method [*Wiemer and Katsumata*, 1999; *Wiemer and McNutt*, 1997; *Wimer and Wyss*, 2000] and minimum misfit between discrete data and synthetic line [*Wiemer and Wyss*, 2000].

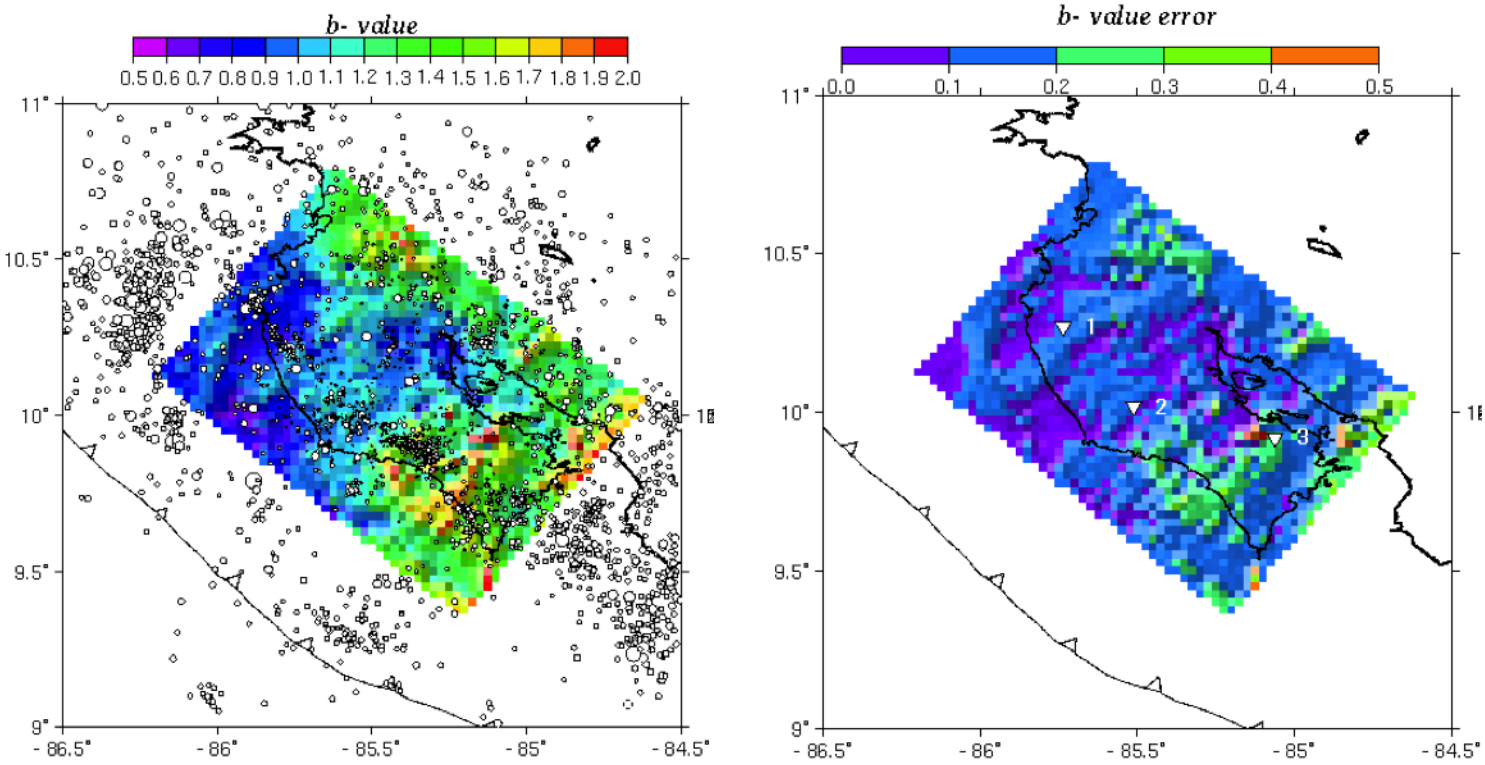


Figure 13. (Left) Spatial distribution of b-values by using LSR and catalog of events without setting the fitting slab. Open circles are earthquakes. (Right) Relevant errors of b-value determined by LSR.

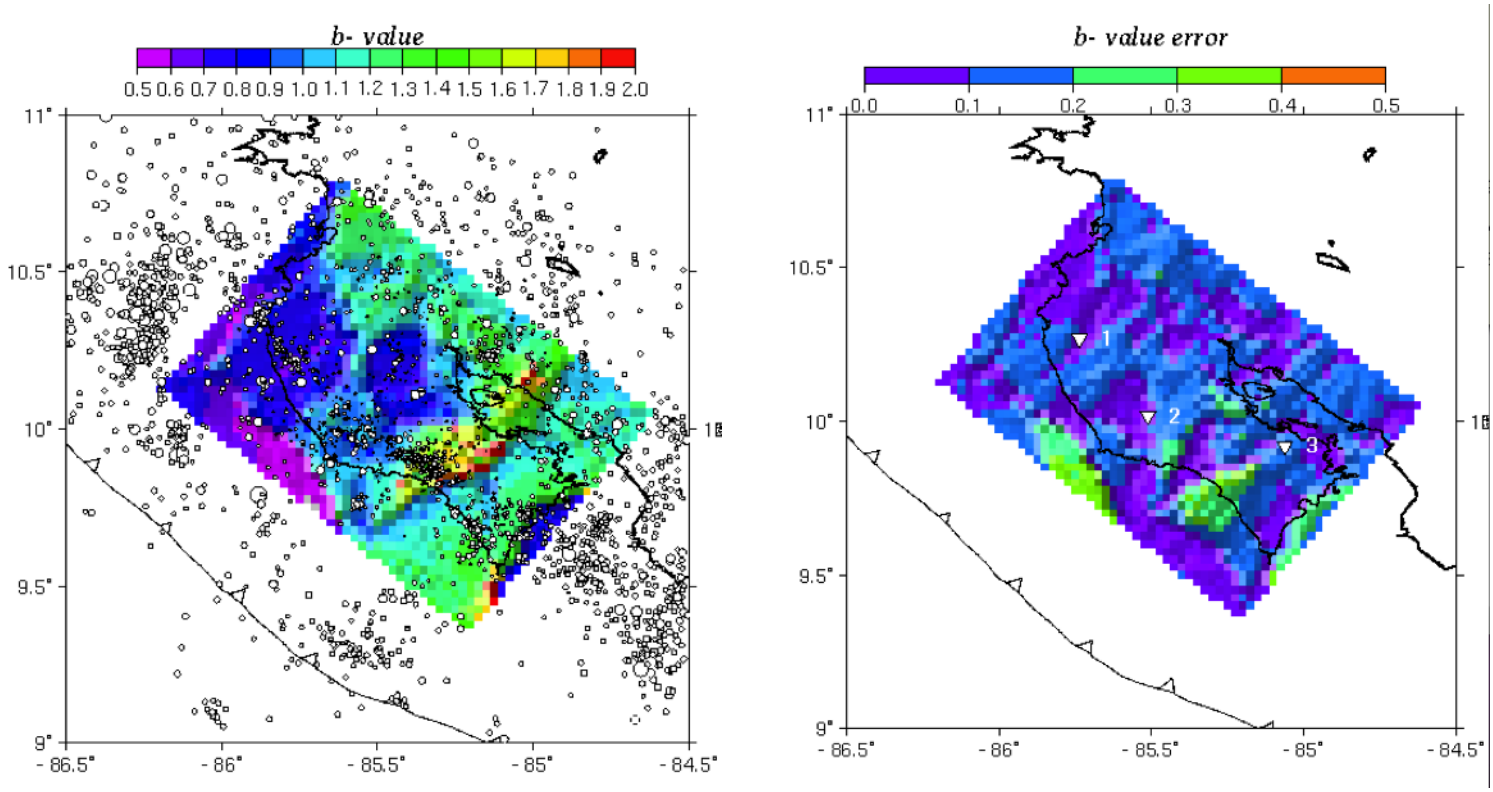

Figure 14. (Left) Spatial distribution of *b*-values by using maximum likelihood method and catalog of events without setting the fitting slab. Open circles are earthquakes; (Right) Spatial distribution of *b*-value errors by using bootstrap sampling method, and same catalog of figure 13

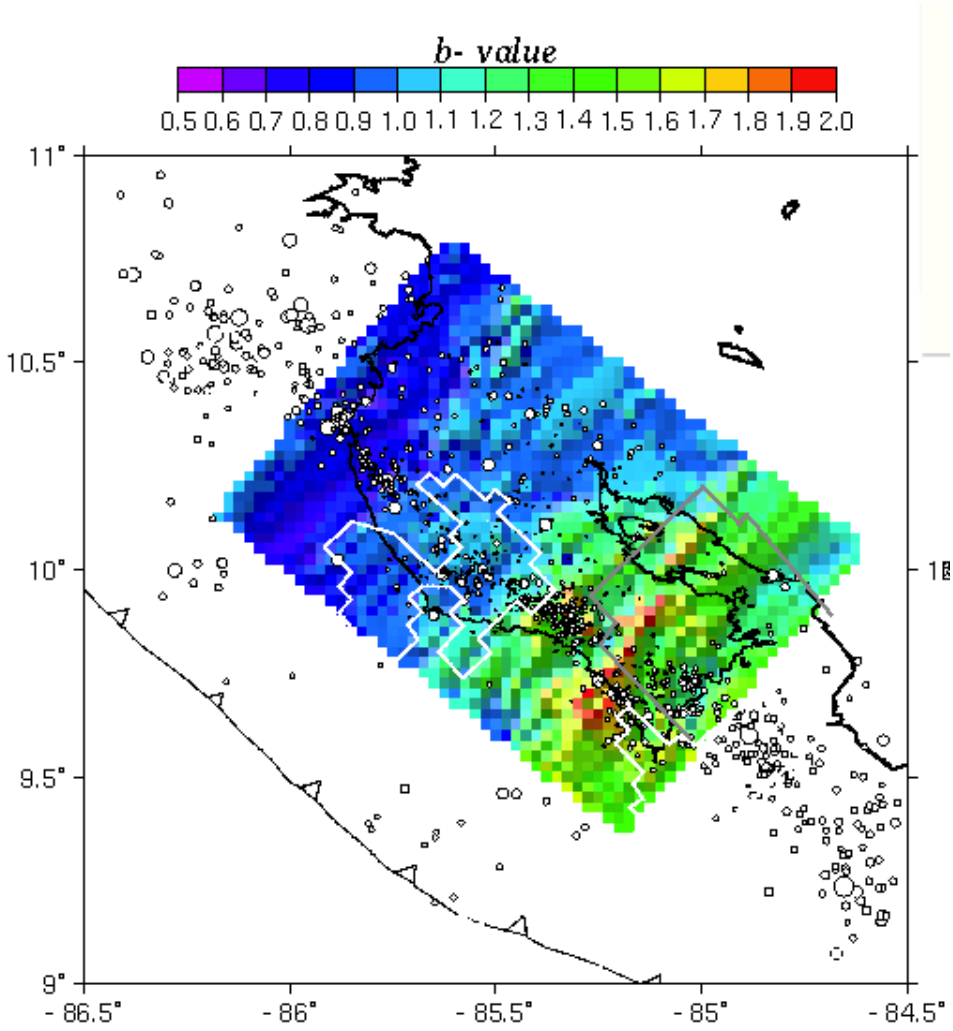


Figure 15. Spatial distributions of *b*-values determined by maximum likelihood method. White contours cover the fully locked interseismic fault patches determined by GPS data from 1996 through 2010 [*Feng et al., 2010 AGU presentation*]. Grey contour covers the maximum slip (~12cm) of slow slip events occurred in May 2007[*Outerbridge et al.*, 2010]

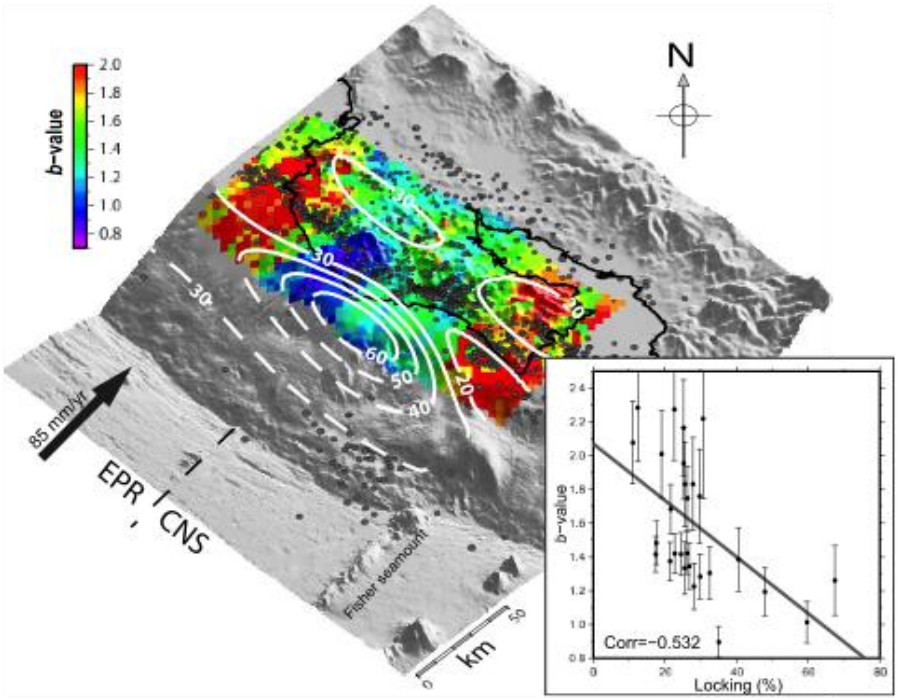


Figure 16. Map of Nicoya FMD determined by MLE and catalog from late 1999 through mid-2001 [*Ghosh et al.*, 2008]. White contours represent relevant locked slip inverted by GPS data between 1994 and 2000 [*Norabuena et al*., 2004]. (inset) The negative correlation between geodetically derived interface locking and *b*-value.[*Ghosh et al*., 2008]

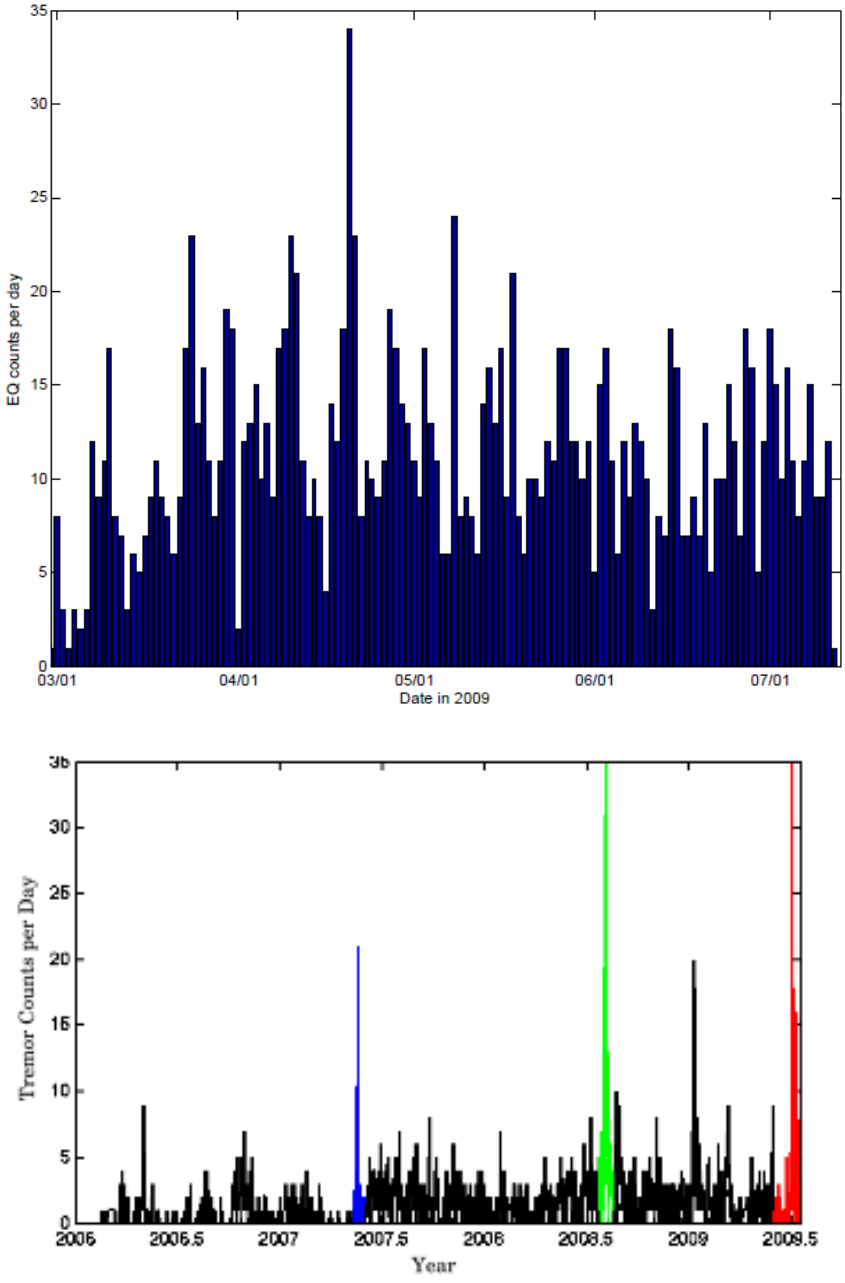


Figure 17. (Up) Earthquake histogram of daily events from March through July 2009 near Nicoya Peninsula. All events are just collected within the fitted slab. (Down) Tremor histogram of daily events from 2006 to mid-2009 [*Walter et al.,* 2010]. Different colors represent three major tremor episodes located near Nicoya. Blue one is May 2007, green one is August 2008, and red one is April 2009.

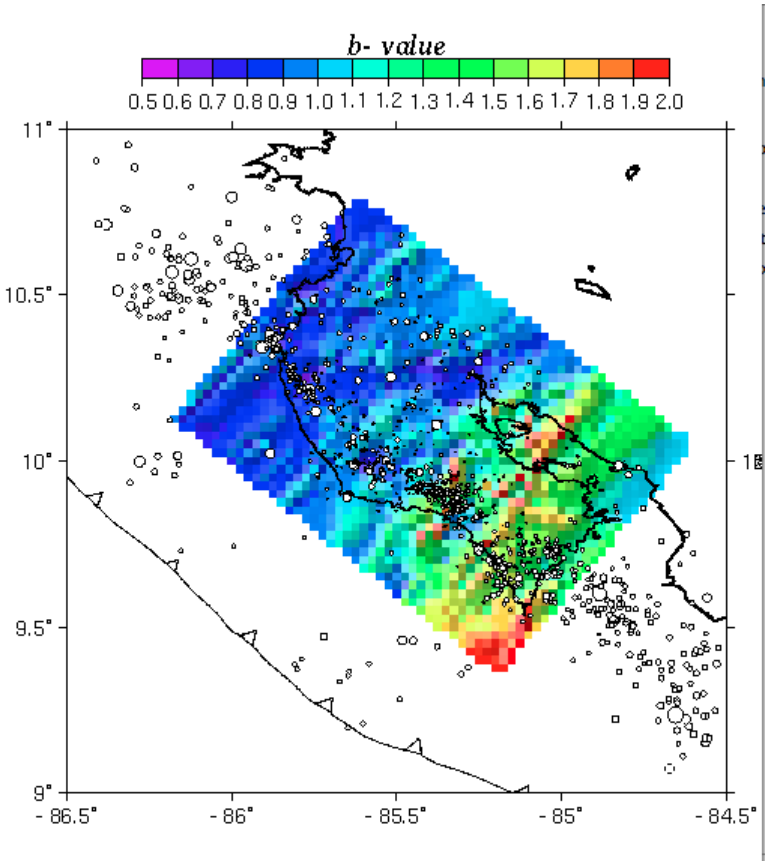


Figure 18. Spatial distributions of b-values by using Maximum likelihood estimation and subset catalog that excludes the events occurred in April 2009.